RSC Advances

PAPER

View Article Online
View Journal | View Issue

Cite this: *RSC Adv.*, 2020, **10**, 42235

TiO_2 Co-doped with Zr and Ag shows highly efficient visible light photocatalytic behavior suitable for treatment of polluted water

M. Aqeel,[a] M. Ikram, *[a] M. Imran,[b] A. Ul-Hamid, *[c] U. Qumar,[d] A. Shahbaz,[e] M. Ikram[f] and A. Saeed [g]

The objective of this study is to analyze the effects of zirconium (Zr) and silver (Ag) doping on the photoactivity of titania (TiO_2). Zr–Ag (ZA) co-doped TiO_2 products were fabricated *via* sol–gel technique and their properties (structural and chemical) were characterized. The weight ratio of TiO_2 was fixed, while weight ratios of Zr and Ag were varied from 2 to 4, 6 and 8 wt% while synthesized samples were calcined at 400 °C for 3 h. The XRD results demonstrated that the incorporation of metal doping agents failed to alter the host material's lattice structure, however, its crystallite size was reduced from 13.54 to 5.05 nm with increasing Zr^{4+} and Ag^{+} concentrations. FTIR spectroscopy was used to examine various functional groups. In the attained spectra, an ample absorption peak between 500 and 1000 cm^{-1} was recorded, which was ascribed to Ti–O–Ti linkage vibration mode present within TiO_2. Surface morphology, microstructure, SAED patterns and elemental composition were examined with FE-SEM, HR-TEM and EDX, which served to confirm the ZA-doped TiO_2 product. Band gap energy of the co-doped material was significantly reduced as indicated by a higher wavelength redshift in the spectra. The photoactivity and kinetics of photo-products were investigated by observing photo-decolorization of methylene blue (MB) under a radiation source. Photodecomposition of MB was dramatically enhanced when titania co-doped with Zr and Ag was employed compared to un-doped or mono-doped TiO_2. The ZA (8 wt%) co-doped TiO_2 photocatalyst depicted the maximum MB removal efficiency (~93%) within 90 min under a light source.

Received 13th October 2020
Accepted 10th November 2020

DOI: 10.1039/d0ra08718a

rsc.li/rsc-advances

1. Introduction

In recent decades, air and water pollution in urban areas produced mainly by automobiles and the chemical industry has become a serious threat to public health. The air pollutants accumulated indoors can cause aiments such as sick building syndrome (SBS) which may prove potentially fatal. Symptoms of SBS include headache, dry cough, dizziness, aggravated asthma, and throat, eye or nose irritation and various diseases produced by water contaminants include typhiod fever, amoebiasis and malaria.[1] Commonly found indoor air pollutants include NO, NO_2, CO, CO_2, VOCs particles and biological contaminants.[2] Bacteria, fungi (including molds) and viruses cause biological pollutants, which affect the respiratory system causing various allergies both in humans and animals. Hazardous chemicals in waste-water also have bad effects on human beings and can damage the nervous system.[3,4] Several approaches have been adopted to remove biological and water pollutants from the environment and household waste-water, respectively. One way is to spray germicides for the prevention of infections, however, chemical residue may pollute the interior environment in this method. To remove biological contaminants from water and air, a useful alternative is photocatalysis, which is carried out in the presence of a photocatalyst and irradiation.[5]

Many articles have reported that metal oxide photocatalysts are potential candidates for photodegradation of environmental organic contaminants. Among the investigated photocatalysts, nanocrystalline TiO_2 (titania) displays highly promising photocatalytic potential for photodegradation of environmetal pollutants, which is ascribed to its inert behavior and non-toxic and good physicochemical stability.[6–8] It is also a cost-effective

[a]*Solar Cell Applications Research Lab, Department of Physics, Government College University Lahore, Punjab, 54000, Paksitan. E-mail: dr.muhammadikram@gcu.edu.pk*
[b]*State Key Laboratory of Chemical Resource Engineering, Beijing Advanced Innovation Centre for Soft Matter Science and Engineering, Beijing Engineering Center for Hierarchical Catalysts, Beijing University of Chemical Technology, Beijing 100029, China*
[c]*Center for Engineering Research, Research Institute, King Fahd University of Petroleum & Minerals, Dhahran 31261, Saudi Arabia. E-mail: anwar@kfupm.edu.sa*
[d]*Department of Physics, Riphah Institute of Computing and Applied Sciences (RICAS), Riphah International University, 14 Ali Road, Lahore, Pakistan*
[e]*Department of Physics, Government College University Lahore, Punjab, 54000, Pakistan*
[f]*Institute of Chemical Engineering and Technology (ICET), University of the Punjab, Lahore 54000, Pakistan*
[g]*Department of Chemistry, Quaid-i-Azam University, Islamabad 45320, Pakistan*

technique to use. Unfortunately, titania depicts photocatalysis only under ultraviolet irradiation due to its wide band energy (~3.2 eV), which suggests that TiO_2 can only utilize 3–5% of incoming solar light. Furthermore, titania shows a high tendency for high electron–hole recombination, which also serves to decrease its photo-activity. It follows from the above that limitations of TiO_2 can be removed by utilization of visible spectrum and inhibition of electron–hole recombination. To improve the photocatalytic performance of TiO_2, first approach is to control the structure of titania particles such as morphology, crystal phase and surface area. Other methodologies include modifying particles of TiO_2, semicondutor coupling, metal/nonmetal ions doping, deposition of nobel metals and dye sensitization.[9,10] Among various TiO_2 modification techniques, metal or nonmetal doping with titania has been widely studied.

Nonmetal doping of TiO_2 can clearly harvest visible light range, however during the anealing process, doped nonmetal content decreases and titania photoactivity is diminished. Fortunately, metal ions doping of TiO_2 could also increase its photoactivity due to its absorption of visible radiation. The quantum efficiency of titania can be improved *via* doped metal ions which reduce probability of recombination of photogenerated pairs (electrons and holes) and act as traps for electrons. This serves to expand absorption range towards visible spectrum and enhance redox potential of photogenerated radicals. Additionally, loss of doped metal content would not take place during anealing process. Therefore, doping of TiO_2 with transition metals have been investigated significantly due to its photoactivities under UV-visible irradiation.[11–14] Currently, some researchers undertook co-doping of titania to enhance photoactivity behavior.[15,16] These studies suggested that improved photoactivity of observed products could be due to a synergetic effect between incorporated metal ions. These research reports revealed that TiO_2 modification *via* co-doping may prove to be an effective technique to enhance photocatalytic activity.

Doping of various novel metals such as Zr,[17] Cr,[18] Pd,[19] Au,[20] Pt[21] and Ag[22] onto TiO_2 have been reported to improve photoactivity of titania under visible radiation. This article will investigate co-doping of TiO_2 with Ag and Zr, as each dopant metal component plays a distinct role in increasing photoactivity. As reported earlier, some co-dopants can boost photocatalytic activity reaction due to synergistic effects. Ag is a commonly recommended dopant for reducing band gap energy, enhancing visible irradiation absorption and decreasing recombination probability of electron–hole pair during photoactivity.[23,24] Addionally, Ag is also a good candidate for antimicrobial performance. Therefore, both photocatalytic and antimicrobial activities could be investigated *via* Ag-doped TiO_2 products under visible light. In addition to Ag, researchers have used Zr as a dopant material for titania. Zr plays an important role in improving stability of anatase phase, increasing surface area, inhibiting recombination centres (electrons and holes) and increasing absorption band towards visible range.[25,26] Although, several research articles on the benefits of doping of titania with Ag and Zr separately have been reported to enhance photoactivity performance but few articles with limited advantages of co-doping of Ag and Zr have been published. Many aspects of Ag and Zr co-doping are still unrevealed and require further investigation.

Thus, this article aims to improve photoactivity efficiency of Zr–Ag co-doped TiO_2 in degrading azo-dye methylene blue (MB) under visible light. A simple sol–gel technique was adopted to fabricate pure titania and co-doped TiO_2 under ambient conditions.[27] The synergistic effects of both incorporated contents (Zr and Ag) on TiO_2 photoactivity were recorded and kinetic reaction of under study materials was also proposed.

2. Experimental details

2.1 Materials

Titanium(IV) butoxide ($Ti(OBu)_4$), silver nitrate ($AgNO_3$) and zirconium acetate ($C_4H_6O_4Zr$) were acquired directly from Sigma-Aldrich (Germany). Methanol (CH_3OH, ≥99.9%) and hydrochloric acid (HCl, 37%) from Merck (Germany) were used as-received. Methylene blue, chemical structure depicted in Fig. 1, and ethanol (C_2H_5OH, 99.8%) were attained from BDH

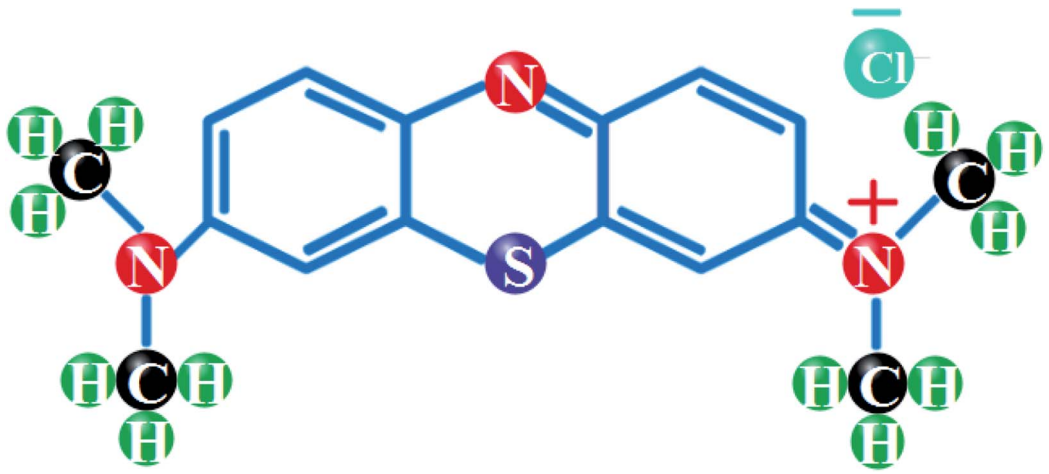

Fig. 1 Structural formula of MB.

(United Kingdom) and local market, respectively. In this research work, all reagents were employed without additional purification.

2.2 Preparation of Zr–Ag/TiO_2 composites

Undoped TiO_2 and Zr–Ag (ZA) co-doped TiO_2 products were fabricated using acid-catalyzed sol–gel technique.[27,28] Briefly, $Ti(OBu)_4$ (10 mL) was poured in methanol (50 mL) while HCl (2 mL) with distilled water (3 mL) was added in titanium solution under continuous stirring. Now, aqueous solutions of various concentrations of silver nitrate/zirconium acetate (2, 4, 6 and 8 wt%) were prepared and added dropwise in titanium solution under vigorous stirring. During fabrication, ethanol aqueous solution was mixed in titanium mixture at 60 °C (2 h) under constant stirring. After gelation, the product was dried at 100 °C (12 h) and in addition, amorphous titania was transformed into crystalline structure *via* muffle furnace at 400 °C (3 h) as depicted in Fig. 2.

2.3 Photoactivity process

The photocatalytic experiments of as-fabricated TiO_2 products were carried out by investigating decomposition rate of a model pollutant (MB) under UV-vis light source (see Fig. 3). Irradiation source used for photoactivity was Philips 400 W high pressure mercury-lamp (luminesce flux ≈ 22 000 lm and bulb temperature max. ≈ 350 °C) which was placed vertically at MB aqueous solution. Details about dye preparation and determination of photo-degradation rate are outlined in previous articles.[29–32] For each experiment, reaction suspension was prepared by mixing 10 mg photocatalyst in a 200 mL glass beaker containing 60 mL MB aqueous solution (MB stock solution = 10 mg L^{-1}). Prior to irradiation, prepared suspension was stirred for 10 min to establish equilibrium between dye particles and photocatalyst surface. After each 20 min, 5 mL degraded solution was withdrawn and employed for UV-vis spectroscopy to estimate MB decomposition from reduction of absorption intensity at λ_{max} = 665 nm. The photoactivity efficiency was calculated *via* the following expression:

$$\text{Degraded efficiency } (\%) = \left(1 - \frac{C}{C_o}\right) \times 100 \quad (1)$$

where C_o and C are before illumination and after MB degradation concentrations, respectively. Control test of MB was also performed under the above-mentioned conditions, however without nanoparticles. To evaluate reusability of nanomaterials, degraded pollutant solution (~decolorized solution) was centrifuged at 6500 rpm (12 min) and induced catalyst was recovered. To reuse photocatalyst again for further MB decomposition tests, recovered nanoparticles were dried in furnace at 70 °C (3 h). Additionally, four cycles of experiments were performed to test durability of catalysts. After each test

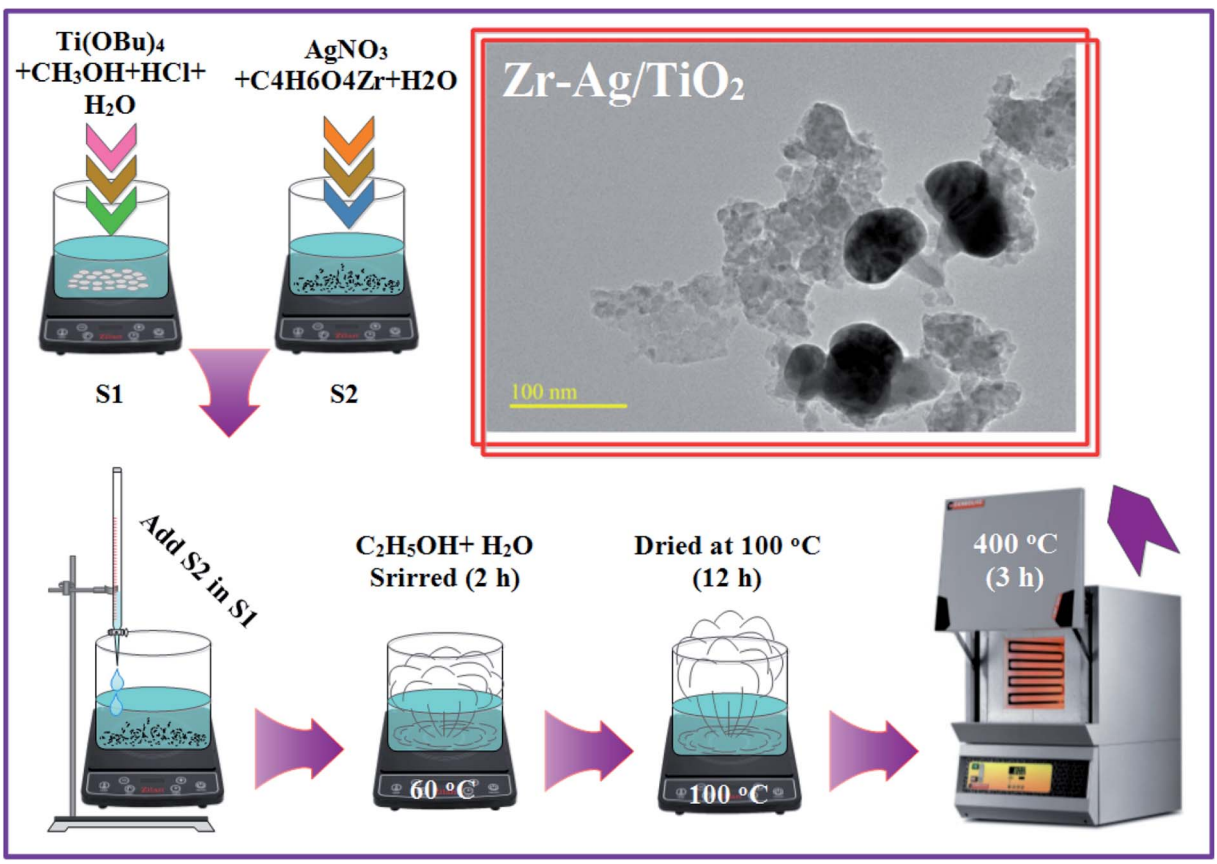

Fig. 2 Schematic illustration of fabrication of Zr–Ag/TiO_2 samples.

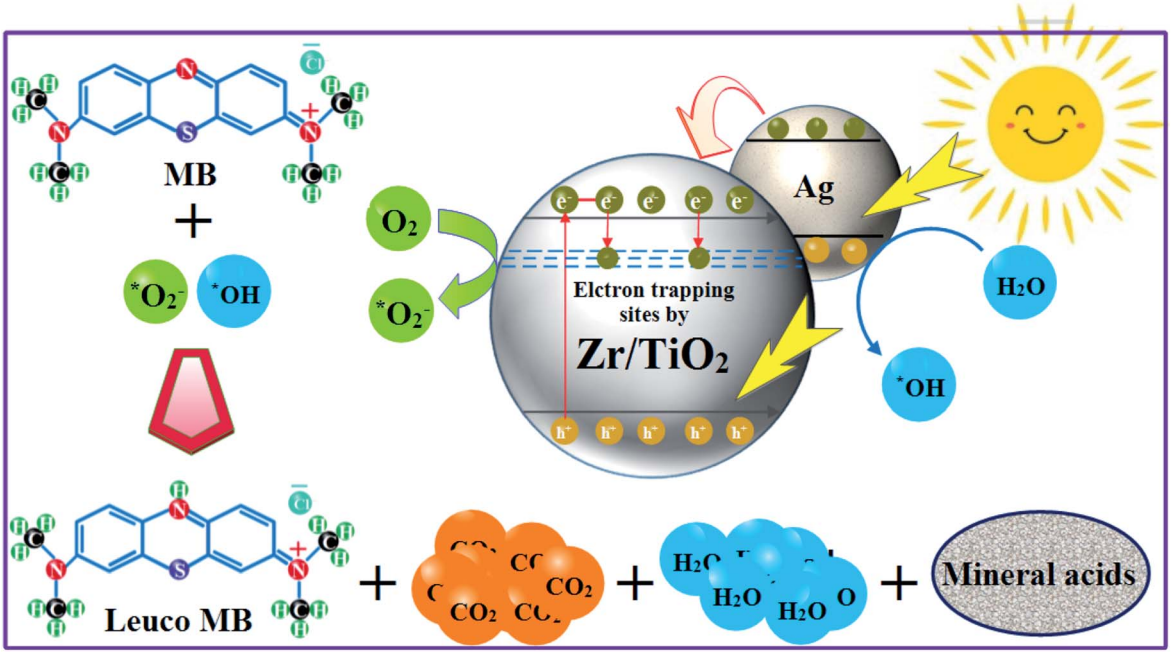

Fig. 3 Photoactivity mechanism of products by harvesting visible light.

cycle, photocatalytic material was centrifuged, heated and used for next photoactivity.

2.4 Kinetic study of photocatalysed decomposition

To quantitatively understand MB degradation reaction kinetics in our photo-experiments, we applied simplified Langmuir–Hinshewood pseudo first-order kinetic model.[33] According to this model (eqn (2)), apparent rate-constant of photoactivity of MB dye at initial quantity (10 mg L^{-1}) can be calculated as:

$$\ln\left(\frac{C_o}{C}\right) = kt \quad (2)$$

where concentrations of contaminant (mg L^{-1}) in water at t_o and t time are C_o and C, respectively and k is apparent first-order reaction rate-constant. At optimum conditions, the recovery and reusability of photocatalysts were also studied.

2.5 Characterization

The fabricated ZA–TiO_2 nanomaterials were subjected to several analytical characterization techniques at room temperature. Structural and phase constitution of Zr and Ag dopants in titania was measured through X-ray diffractometer (XRD) of PANanlytical-Xpert-PRO machine equipped with K_α-radiation of Cu (λ = 1.54 Å) ranged from 2θ = 10–80°. Functional groups were recorded with FTIR (Fourier transform infrared) spectrometer (PerkinElmer). Structural vibrations of products were examined using Raman microscope (DXR Thermo Scientific) with laser irradiation (532 nm and 6 mW). To analyze light absorption behavior, photoluminescence (PL) and UV-vis images of as-prepared nanostructures were achieved using JASCO-FP -8300 PL machine and Genesys 10S instrument, respectively. Surface morphology and precise amount of dopant in titania nanoparticles were obtained through JEOL JSM-6610LV FE-SEM equipped with energy-dispersive X-ray (EDX) and X-ray fluorescence (XRF) analyzer. HR-TEM (JEOL JEM 2100F) was employed to detect lattice fringes with diffraction patterns, d-spacing between material's planes and surface morphology of nanoparticles.

3. Results and discussion

XRD patterns obtained from pure titania and co-doped ZA/TiO_2 particles fabricated *via* sol–gel technique are displayed in Fig. 4a. In all products, single (anatase) phase of TiO_2 was confirmed through peaks at 2θ = 25.59 (101), 37.93 (004), 48.14 (200), 53.71 (105), 55.06 (211), 62.71 (204), 68.89 (116), 70.24 (220) and 75.05 (215) which well matched with JCPDS file: 021-1272 (ref. 34) while no peaks related to Zr and Ag were identified in any analyzed samples attributed to their low doped quantities. Furthermore, dopant materials did not alter the structure of host material and diffused well within titania lattice, thus increasing visible light absorbance. Major peaks exhibited broadness with increasing doping quantity which may be attributed to the presence of lattice strain in synthesized samples resulting in a decrease in crystallinity.[35] The crystallite size of as-prepared products was calculated *via* Debye–Scherer equation:

$$D = \frac{0.9\lambda}{\beta \cos\theta} \quad (3)$$

where D denotes crystallite size, λ stands for X-ray wavelength and β presents full-width at half-maximum (FWHM) of the most intense peak (101). The crystallite size decreased with increasing dopant quantity and ranged from 13.54–5.06 nm.

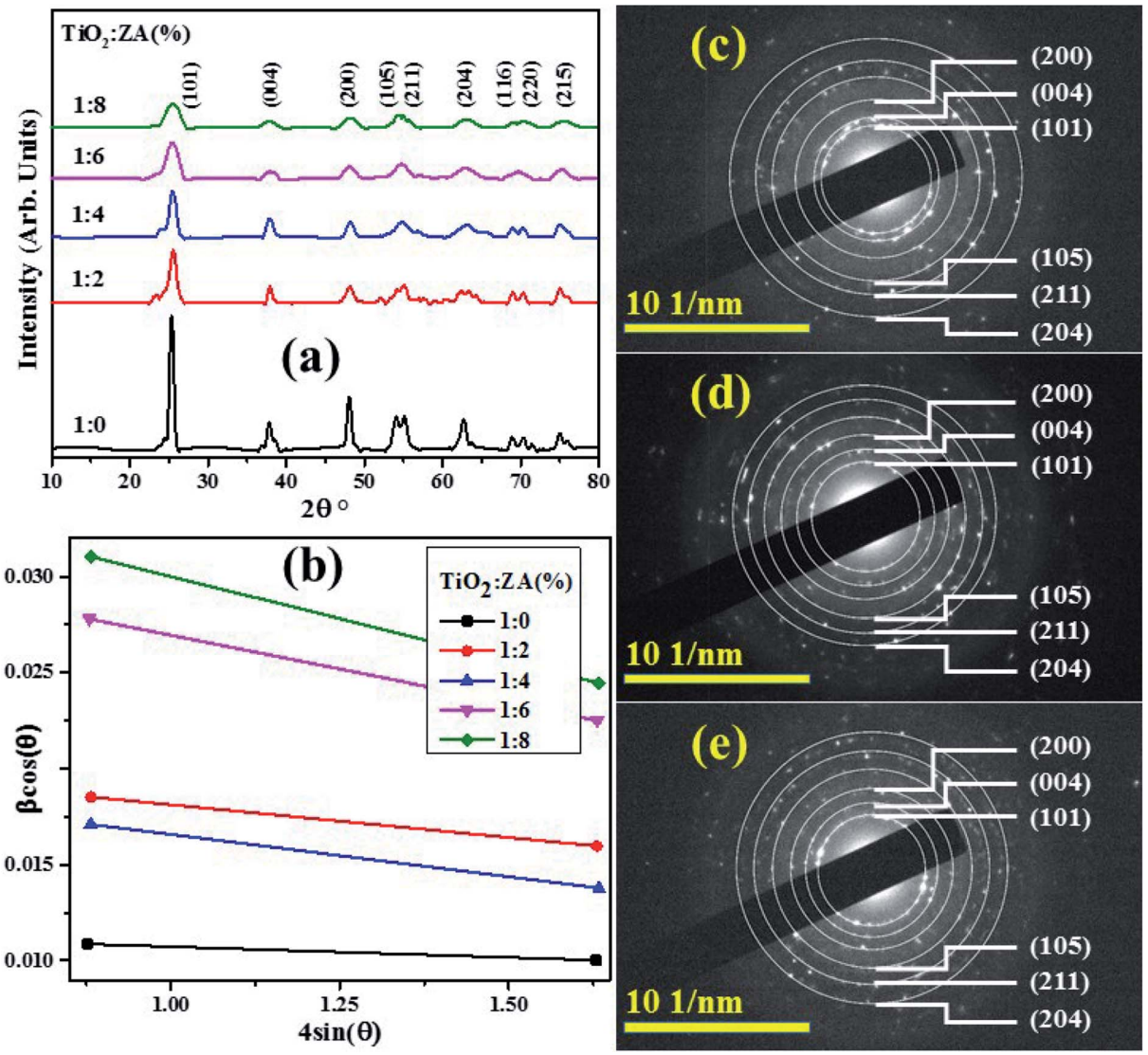

Fig. 4 (a) XRD spectra, (b) Williamson–Hall plots of pure and ZA-doped TiO_2 (c–e) SAED profiles of undoped, 4 and 8 wt% doped TiO_2 samples, respectively.

The crystallite size and strain broadening of prepared nanostructures can also be attained using Williamson–Hall (WH) relation[36] as indicated in eqn (4).

$$\frac{\beta \cos(\theta)}{\lambda} = \frac{k}{D_{WH}} + \frac{4\varepsilon \sin(\theta)}{\lambda} \quad (4)$$

where β indicates full-width at half-maximum (FWHM), θ is diffraction angle, k denotes shape factor, ε stands for strain, λ is wavelength of Cu Kα and D_{WH} presents crystallite size. Graph was plotted between $\beta \cos(\theta)$ *vs.* 4 $\sin(\theta)$ attaining straight line (Fig. 4b) whose *y*-intercept provided crystallite size and slope of straight line indicated strain. Estimated average crystallite size and strain of pure titania and co-doped TiO_2 composites are illustrated in Table 1. The results clearly show that estimated mean crystallite size *via* W–H plot are well consistent with calculated results from Scherrer relation. All titania samples showed negative strain values, pure titania contained maximum strain value and strain value decreased upon doping of Zr and Ag. Fig. 4c–e depict selected area electron diffraction (SAED) patterns of nanostructures with six concentric circles indexed as (101), (004), (200), (105), (211) and (204) planes which are well matched with XRD analysis and confirm anatase crystal lattice of TiO_2.

Table 1 Calculated mean crystallite size and strain

	Crystallite size (nm)		
Sample	Scherrer method	W–H method	Strain
1 : 0	13.54	12.62	−0.00058
1 : 2	9.08	7.13	−0.00342
1 : 4	8.19	6.59	−0.00443
1 : 6	6.57	4.07	−0.00707
1 : 8	5.06	3.57	−0.00877

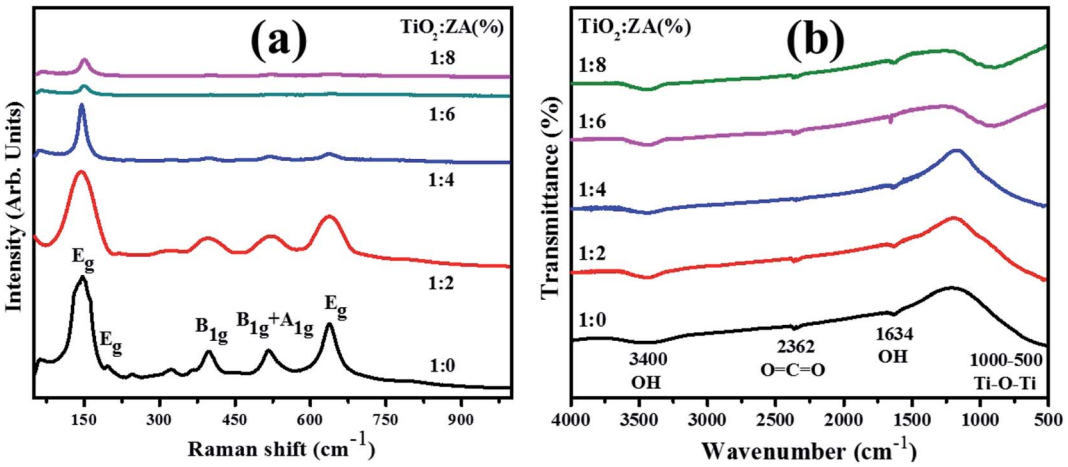

Fig. 5 (a) Raman spectra and (b) FTIR profiles of TiO_2 and co-doped TiO_2 products.

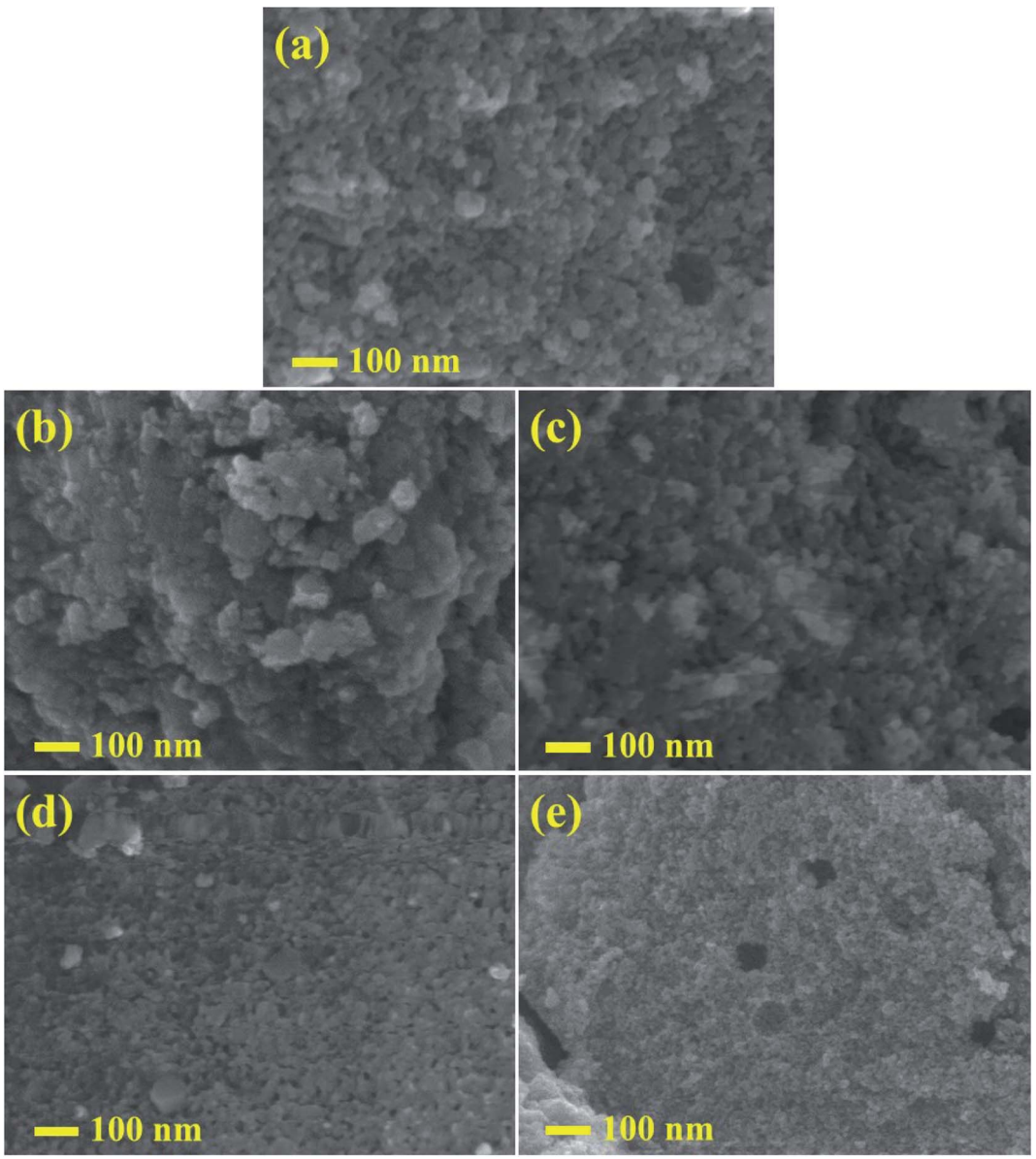

Fig. 6 (a–e) FESEM images of pure and ZA (2, 4, 6 and 8 wt%) doped TiO_2 nanostructures, respectively.

Investigation of structural fingerprints and determination of various molecular vibrational modes in pure and ZA-doped TiO_2 nanoparticles were accessed through Raman spectroscopy (Fig. 5a). Anatase TiO_2 exhibits six active Raman modes which is in line with the analysis reported by Choi *et al.*[37] These modes are illustrated by the following equation:

$$\text{Modes} = (A_{1g} + 2B_{1g} + 3E_g) \quad (5)$$

These six modes and their positions are E_g (144 cm^{-1}), E_g (197 cm^{-1}), B_{1g} (399 cm^{-1}), A_{1g} (513 cm^{-1}), B_{1g} (519 cm^{-1}) and E_g (639 cm^{-1}), respectively. These six modes identified in Raman spectra of host and co-doped TiO_2 nanoparticles harmonize well with the reported literature.[38–40] It is worth mentioning that upshifting and slightly higher wavelength shift in Raman spectra upon incorporation of dopants were detected. Further, Raman intensities from pure to co-doped samples decrease, which correlate with XRD data that indicated decreasing crystallite size as cited previously. Various factors influence the vibrational properties of the prepared product when reduction in crystallite size towards nanometer scale occur.[41]

The first effect relates to volume contraction due to size encouraged radial pressure within nanoparticles. As a consequence, increment in force constant (k) is perceived due to drop in interatomic distances. In case of vibrational transitions, variation in wavenumber is roughly proportional to $K_{1/2}$. Thus, upshifting in Raman bands is detected due to increment in k. Secondly; effect of contraction incorporates diminution in vibrational amplitude of nearby bonds that can be considered as an extent of thermal vibrational as well as static disorder of prepared product. Conclusively, reduction in vibrational amplitude corresponding to crystallite size causes to influence the intensity of Raman modes. Therefore, in view of above discussion it can be concluded that distinction in Raman spectra of host and ZA–TiO_2 nanoparticles appears owing to the impact of decrease in crystallite size on vibrational amplitudes as well as force constant of nearby bonds.[37,42,43]

FTIR spectra were recorded, as presented in Fig. 5b, in the range of 4000–500 cm^{-1} to observe reaction intermediate and functional groups behavior present in fabricated specimens. A broad peak appeared at 3400 cm^{-1} typically assigned to O–H stretching vibration and a small band at 1634 cm^{-1} ascribed to hydroxyl group bending vibration of chemically absorbed H_2O molecules.[44] The hydroxyl group present in samples plays a key role in enhancing photoactivity since these groups react with photogenerated electron–hole pairs and convert into radicals (*OH) required for the removal of MB (as discussed in later section). The band about 2362 cm^{-1} was ascribed to stretching

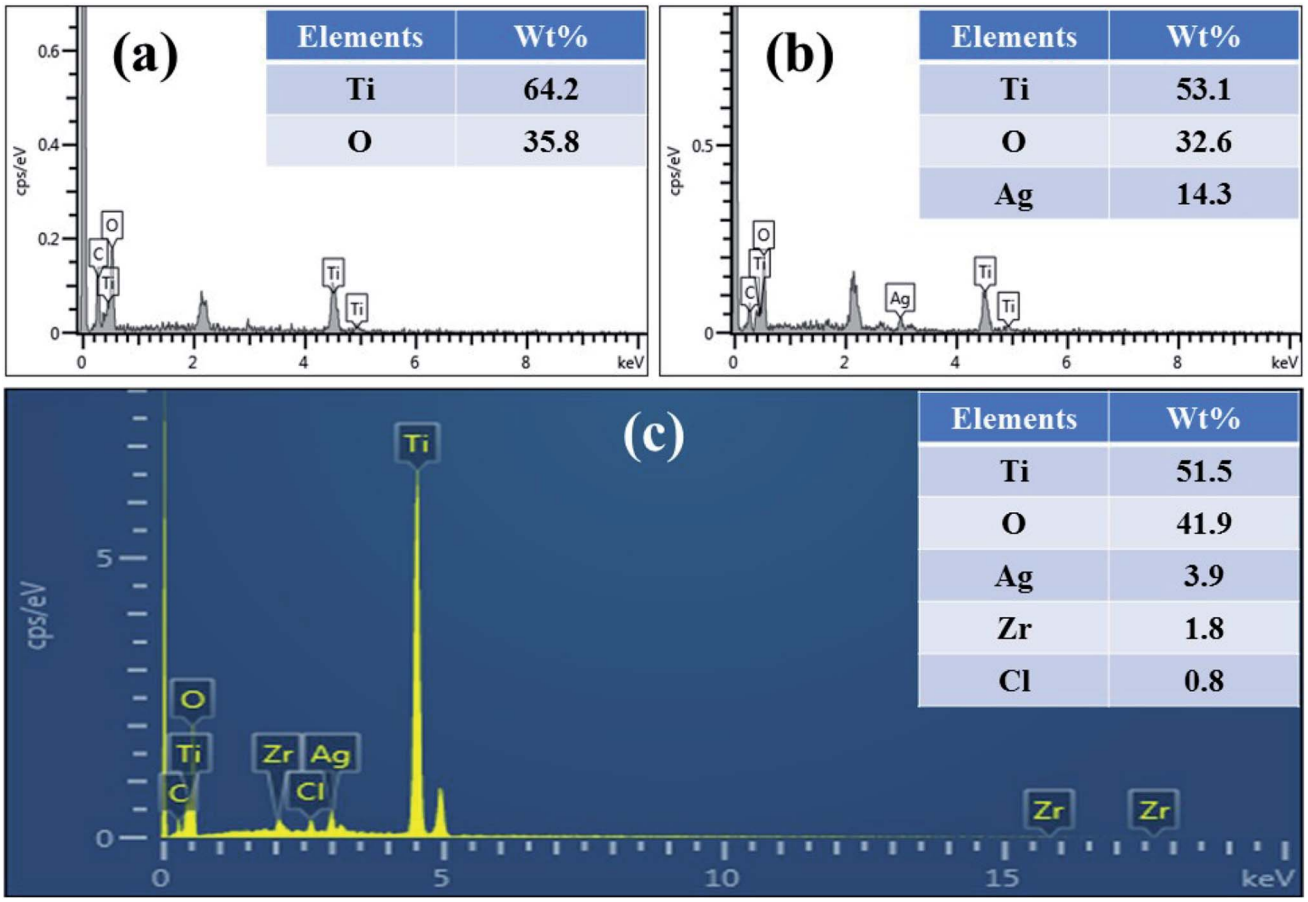

Fig. 7 (a) EDX spectrum of titania and (b and c) EDX profile and XRF pattern of ZA (6 wt%) co-doped TiO_2, respectively.

of O=C=O bonds.[45] An ample absorption band in recorded spectra from 500–1000 cm^{-1} corresponded to vibration modes of Ti–O–Ti which confirms metal oxygen bonding.[46,47]

Micrographs of undoped and doped samples at a magnification of 100 000 were obtained through FE-SEM as depicted in Fig. 6. Large agglomerations of particles were observed in TiO_2 as shown in Fig. 6a, whereas with the incorporation of ZA (2, 4, 6 and 8) wt% in TiO_2 (Fig. 6b–e), nanoparticles consisted of agglomerated particles with small particles size. The FESEM observations and XRD calculations confirmed that the presence of Zr and Ag had restricted increase in particle size of titania. ZA-doped TiO_2 displayed uniform round shape with fine particles and good dispersion. The micromorphology of prepared samples was further characterized using HRTEM analysis.

To examine the chemical composition of particles precipitated on the surface of TiO_2, EDX analysis was performed (Fig. 7a and b). The elemental analysis confirmed that products were composed of Ti, O, C and dopant materials. In given spectra, peak of C appears due to carbon tab used to support the samples. EDX spectrum of 1 : 6 sample clearly revealed that TiO_2 specimen possessed Ti, O and Ag only with weight% of 53.1, 32.6 and 14.3%, respectively. Although, XRD spectra could not evidently confirm Zr and Ag in doped products, EDX images confirmed the existence of dopant materials in TiO_2 lattice. XRF spectroscopy was used to probe actual concentration of elements in ZA-doped TiO_2 nanocomposite. Based on XRF results (Fig. 7c), as-fabricated sample contained Ti (51.5 wt%), O (41.9 wt%), Ag (3.9 wt%) and Zr (1.8 wt%). It is notable that recorded concentrations were very close to predetermined values of 1 : 6 sample.[48] In the present study, XRF technique represented the actual composition more accurately compared to EDX.

A common feature of sol–gel method is agglomeration and larger than 2 μm agglomerated particles of titania have been reported.[49] The micromorphology of prepared samples was further characterized using HRTEM analysis. HRTEM images with high resolution and lattice fringes patterns of undoped, 4 and 8 wt% doped nanoparticles are presented, respectively in Fig. 8. The HRTEM micrograph (Fig. 8a) elucidates non-uniform agglomerated nanocrystalline micrograph of TiO_2 with nearly spherical shape. Upon doping with Zr and Ag, nanostructures get slightly scattered with random distribution and

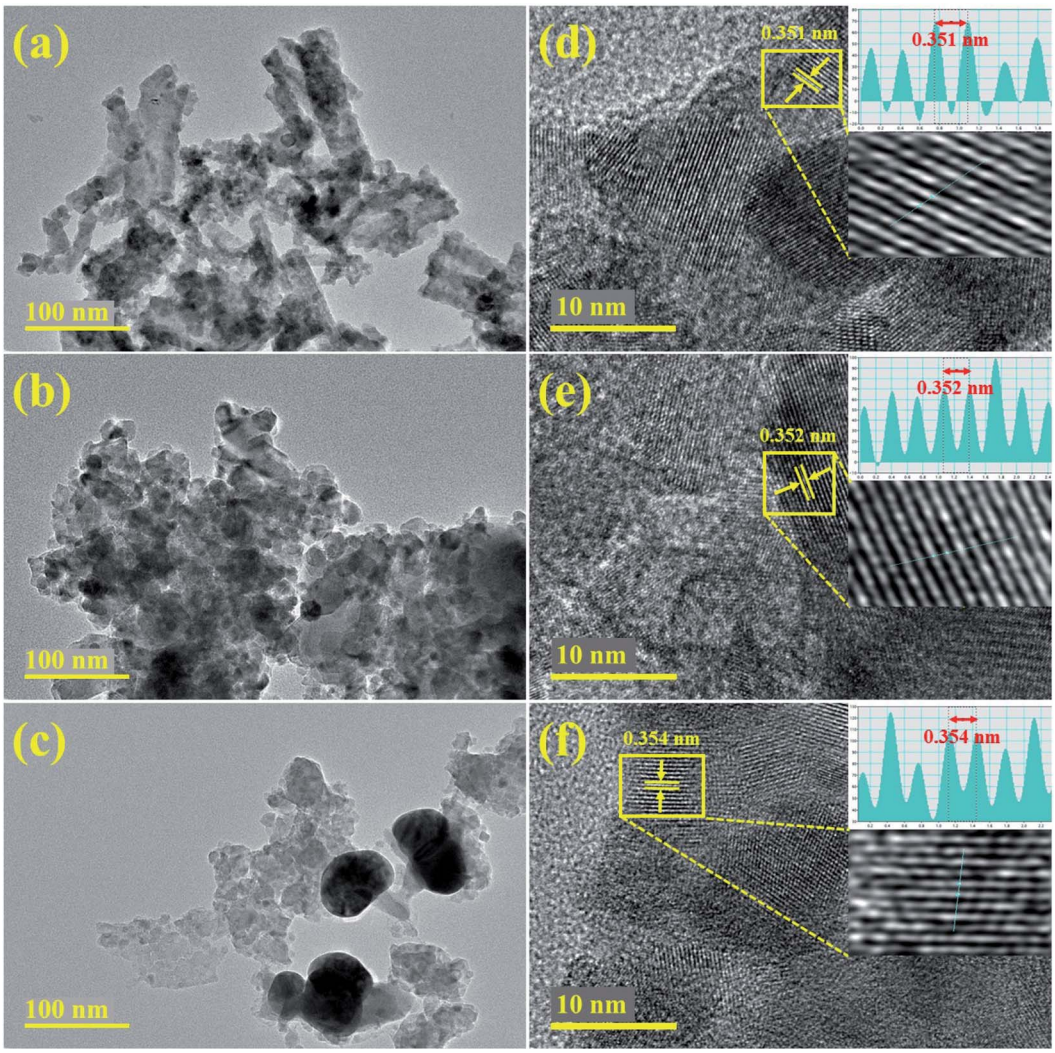

Fig. 8 (a–c) HRTEM and (d–f) lattice fringes of undoped and ZA (4 and 8 wt%) doped TiO_2 fabricated samples, respectively.

agglomeration is reduced along with slight transparency of nanostructures (Fig. 8b and c). Titania doped with maximum Zr–Ag quantities depicted random distribution of stone-like structures and chunky areas with agglomeration. Furthermore, to obtain detailed information about interplanar distance and morphology of samples, HRTEM patterns up to 10 nm were recorded as represented in Fig. 8d–f. Well-ordered distinct atomic planes with O–Ti–O arrangement and periodic arrangement of atoms at specific areas can be observed on a single grain, where interplanar distance was measured about 0.351 nm for pure titania (Fig. 8d). In Fig. 8e and f, with the incorporation of Zr and Ag, *d*-spacing of nanostructures was slightly widened and observed from ~3.52 to 3.54 nm. According to lattice fringe images, these periodic arrangements match with lattice spacing of (101) plane of anatase (TiO_2) phase and are consistent with XRD analysis.[50,51]

UV-vis spectroscopy was employed to analyze interactions of nanoparticles with photon energies. Absorbance spectra of pure titania and ZA (2, 4, 6 and 8 wt%) doped TiO_2 nanomaterials are illustrated in Fig. 9a. The absorbance spectrum of TiO_2 has single absorption band usually ascribed to photon excitation from valence (generally generated by oxide anion's 2p orbitals) to conduction band (usually formed *via* Ti^{4+} cation's $3dt_2g$ orbitals).[52] The absorption band for undoped titania was recorded at 300–330 nm and an optical absorption edge shift for doped titania products towards visible region was observed. Obviously, this redshift originates from TiO_2 band gap narrowing due to the addition of dopant materials. In doped TiO_2 products, addition of Ag ions produces significant change in TiO_2 absorbance spectrum resulting in absorption edge spectra from 332 nm to visible area.[53–55] This visible region absorption of doped titania depicts possibility of lower energy transitions since, metal clusters enhance localized energy levels of TiO_2 band gap into which titania valence band electrons are excited longer than 332 nm wavelength. The redshift and decreased band gap of doped sample may result from defects attributed to Zr^{4+} trace quantities in TiO_2 host lattice.[56] The band gap energy of studied samples was calculated by following Tauc's equation:

$$\alpha h\nu = K(h\nu - E_g)^n \quad (6)$$

where α denotes absorption coefficient, h stands for Planck's constant, ν depicts frequency and K exhibits absorption index. The difference in band gap of nanomaterials corresponds to difference in products absorption edge wavelength. Electronic transitions between dopant materials and valence/conduction band clearly shift light absorption towards visible region. Absorption edge of pure titania is approximately at 332 nm and

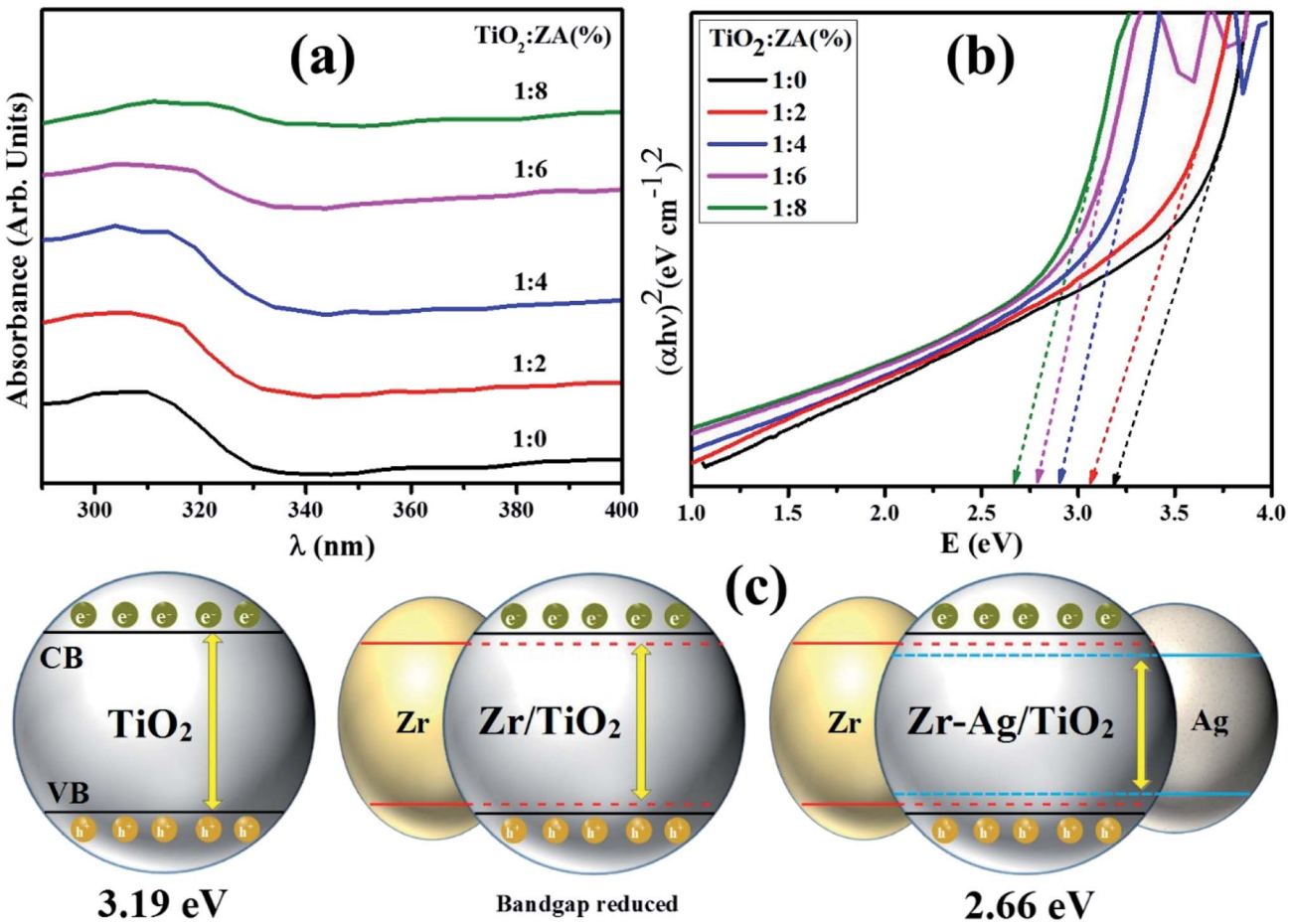

Fig. 9 (a) Absorption spectra, (b) optical band gap energy of synthesized nanomaterials and (c) structural representation of band gap.

the calculated band gap is 3.19 eV.[57] Absorption edge of ZA (8 wt%) doped TiO_2 sample presents largest light absorption with 2.66 eV band gap energy (Fig. 9b) among all prepared nanostructures due to electronic properties of Zr^{4+} and Ag^{+} ions. Therefore, best photoactivity can be achieved *via* 1 : 8 sample of titania, structural representation of band gap has been illustrated in Fig. 9c.

The photocatalytic reactivity of pure titania, Zr–TiO_2 (for sake of comparison, Zr (2 wt%) doped TiO_2 was also included) and ZA (2, 4, 6 and 8 wt%) co-doped TiO_2 were investigated *via* decomposition of dye (MB) under irradiation source after adsorption/desorption was attained in dark for 10 min. Decolorization behavior was analyzed by plotting graph between MB concentration (C/C_0) and irradiation time as presented in Fig. 10a. Under light source, all undoped and doped samples of titania evidently degraded MB within 90 min, while pure TiO_2 sample had the lowest degraded efficiency (23.3%) as depicted in Fig. 10b. Interestingly, ZA (8 wt%)-doped TiO_2 specimen revealed maximum degradation% (92.9%). Therefore, this result identified 1 : 8 nanomaterial as a promising irradiation responsive photocatalyst. When ZA co-doped TiO_2 was activated under light source, electrons transferred from valence band (vb) to conduction band (cb) of induced Ag particles, producing

Table 2 The evaluation of pseudo-first-order kinetic and MB degradation% of photocatalysts

Samples	Degradation%	Kinetic constant $(min)^{-1}$
1 : 0	23.3	0.032
Zr/TiO_2	51.4	0.074
1 : 2	64.1	0.105
1 : 4	74.7	0.145
1 : 6	88.0	0.233
1 : 8	92.9	0.276

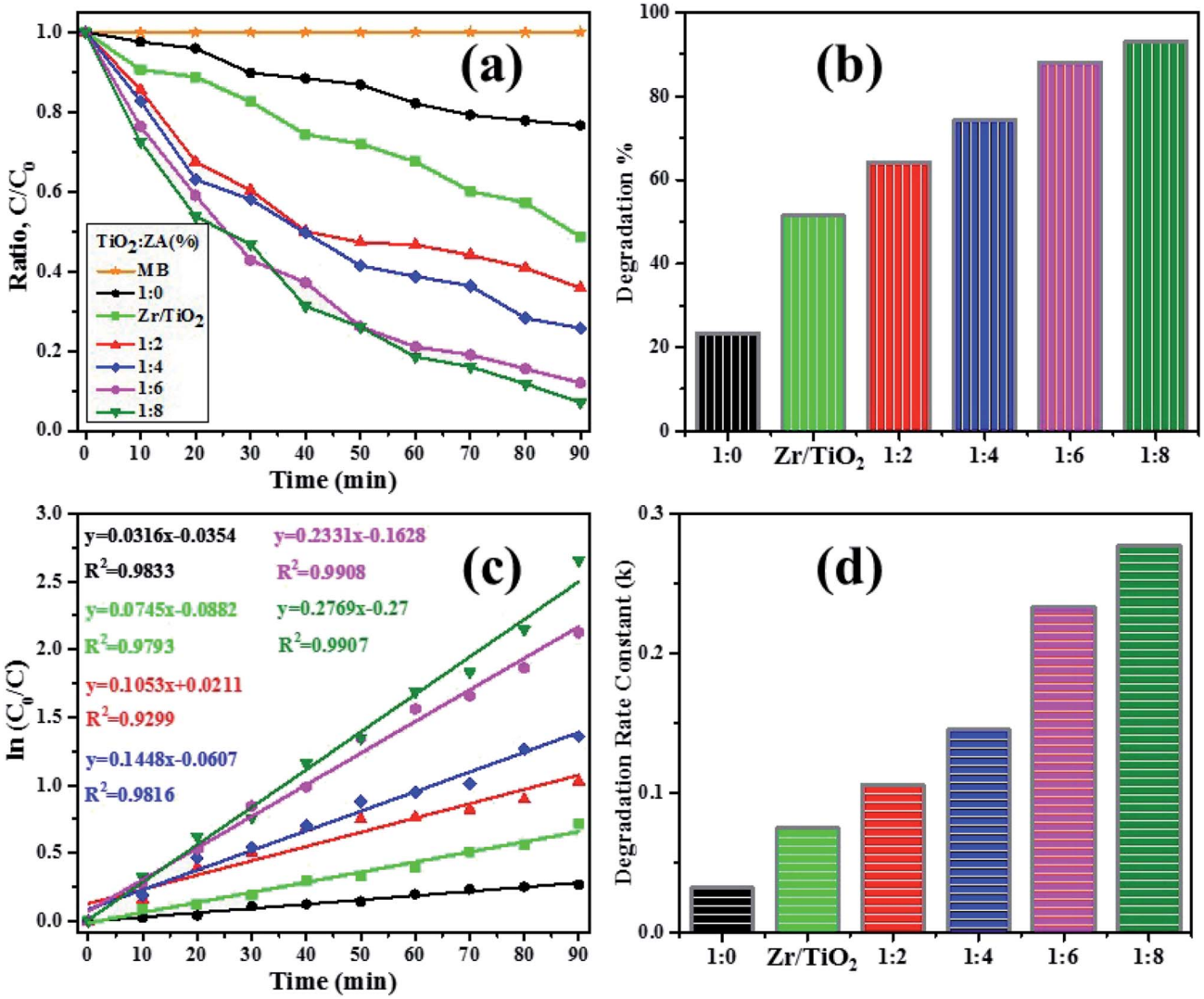

Fig. 10 (a) C/C_0 *vs.* irradiation time plot, (b) degradation% graph, (c) ln(C_0/C) *vs.* illumination time plot and (d) calculated degradation rate constant (k) *vs.* synthesized samples bar graph.

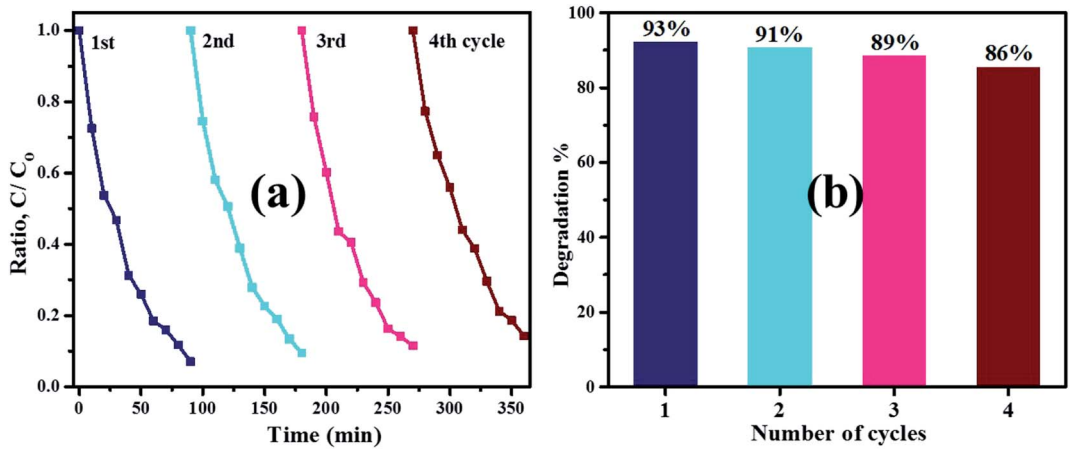

Fig. 11 (a) ZA (8 wt%) co-doped TiO_2 photocatalyst reusability and (b) degradation% bar graph.

electron–hole pairs.[58,59] The Ag cb electrons migrated to cb of doped titania, MB was simultaneously photo-sensitized, and migrated cb electron were injected into cb of doped titania. Following this, oxygen molecules (O_2) were reduced by migrated electrons into active oxygen radicals (O_2^*), and vb of Ag particles reacted with water molecules (H_2O) to produce hydroxyl radicals (OH*). Finally, produced radicals (O_2^* and OH*) attacked MB molecules. Degradation mechanism is illustrated as follows.[60,61]

$$\mathrm{MB} + h\nu \rightarrow \mathrm{MB}^* \quad (7)$$

$$\mathrm{MB}^* + \text{doped } \mathrm{TiO_2} \rightarrow \mathrm{MB} + {}^{\bullet} + \text{doped } \mathrm{TiO_2}\ (\mathrm{e}) \quad (8)$$

$$\text{Doped } \mathrm{TiO_2}\ (\mathrm{e}) + \mathrm{O_2} \rightarrow \mathrm{O_2^{-*}} \quad (9)$$

$$\mathrm{O_2^{-*}} + \mathrm{H^+} \leftrightarrow \mathrm{HO_2^*} \quad (10)$$

$$\mathrm{HO_2^*} + \mathrm{HO_2^*} \rightarrow \mathrm{O_2} + \mathrm{H_2O} \quad (11)$$

$$\mathrm{e^-} + 2\mathrm{H^+} + \mathrm{O_2^{-*}} \rightarrow \mathrm{H_2O_2} \quad (12)$$

$$\mathrm{e^-} + \mathrm{H_2O_2} \rightarrow \mathrm{OH^-} + \mathrm{OH}^* \quad (13)$$

$$\mathrm{MB^{+*}} + \mathrm{O_2}\left(\mathrm{O_2^{-*}}\ \text{or}\ \mathrm{OH^*}\right) \rightarrow \mathrm{CO_2} + \mathrm{H_2O} + \text{other products} \quad (14)$$

As a result, molecules of dye were decomposed and by-products were produced as discussed in above equations. Therefore, photoactivity of photocatalysts was significantly enhanced upon doping. The roles of Ag material also involved decreasing band gap and increasing charge separation.[62,63] On the other hand, Zr particles trapped electrons and reduced the probability of electron–hole pairs recombination. The photodegradation of MB under irradiation with ZA–TiO_2 photocatalysts was attributed to the synergistic effect of both Zr and Ag dopants For example, the degradation% of 1 : 8 photocatalyst reached up to 93% which was higher than pure (23.3%) and Zr–TiO_2 (51.4%). Degradation efficiency of ZA (2 wt%) co-doped TiO_2 (64.1%) was also greater than Zr (2 wt%) doped TiO_2 (51.4%), which is attributed to the presence of both dopants. In addition, surface area of catalyst also affects photodecomposition behavior of MB.[64–66] Furthermore, MB degradation kinetics were analyzed using pseudo-first-order reaction as revealed in above eqn (2). Pseudo-first-order models were plotted between $\ln(C_0/C)$ *vs.* time using eqn (2) as shown in Fig. 10c and calculated degradation rate constant (k) of specimens are also exhibited in Fig. 10d. The calculated k values of TiO_2 and doped TiO_2 under light source are represented in Table 2. Rate constants and dye photodegradation values of co-doped titania achieved significant improvements.

To evaluate steadiness and reusability, the 1 : 8 sample was further used up to four times under irradiation source exposure to photo-decompose MB dye from polluted water. The Fig. 11a illustrates that after four sequential cycling experiments, photocatalyst turns off MB colorant degradation under identical conditions. Degradation efficiency of sample decreased from 93% to 86% after four cycles (Fig. 11b) ascribed to some loss of nanomaterial through washing or centrifugation during recycling tests. According to observed recycling results, the product remained relatively stable and showed significant potential for treatment of hazardous water.

4. Conclusion

Pure and co-doped TiO_2 nanomaterial with Zr and Ag were successfully fabricated *via* sol–gel process and as-prepared products were studied using several characterization techniques. XRD spectra revealed anatase phase formation with broadness of bands upon doping suggesting decrease in crystallinity which may be due to the presence of lattice strain in fabricated nanostructures. Crystallite size of titania samples were also reduced (from 13.54 to 5.06 nm) with doping of Zr and Ag as calculated using Scherrer method. All recorded functional groups belonged to samples under investigation and the presence of typical absorption band at 500–1000 cm^{-1} was ascribed to vibration modes of Ti–O–Ti linkage in titania nanomaterials that depicted formation of pure titania nanoparticles as indicated in FTIR profiles. Nearly spherical morphology of

nanomaterials with high degree of agglomeration could be visualized using FE-SEM and HR-TEM images while *d*-spacing of pure and highest doped TiO_2 was measured at 0.351 and 0.354 nm, respectively. Upon doping, absorption edge moved towards higher wavelength and calculated band gap decreased from 3.19 to 2.66 eV, which corresponded to electronic properties of Z^{4+} and Ag^{+}. MB degradation by TiO_2 under light source was enhanced upon incorporation of Zr and Ag. The ZA (8 wt%) co-doped TiO_2 exhibited synergistic effects during MB photodecolorization under light-source, with highest photodegradation efficiency recorded at about 93%. Ag and Zr doping contents promoted photoactivity by reducing band gap width and decreasing recombination probability of charge carriers (electron–hole pairs), respectively. Therefore, photodegradation ability of ZA (2 wt%) co-doped TiO_2 (~64%) was also higher than Zr (2 wt%) doped TiO_2 (~51%) ascribed to the above-mentioned synergistic effects of dopants.

Authors contributions

M. Ikram designed the research and AS, MA conducted experiments, analyzed the data, and wrote the manuscript. MI facilitated for different characterizations and reviewed the manuscirpt. AUH performed EDS, SEM and HRTEM and reviewed the manuscript. AS, MI and A. Saeed participated in discussion and reviewed the manuscript. All authors read and approved the manuscript for submission.

Conflicts of interest

There are no conflicts of interest to declare.

Acknowledgements

The authors are grateful to the financial support by the Higher Education Commission Pakistan through start research grant project # 21-1669/SRGP/R&D/HEC/2017. Support provided by the Research Institute, King Fahd University of Petroleum & Minerals, Dhahran, Saudi Arabia is also appreciated.

References

1 S. M. Joshi, The sick building syndrome, *Indian J. Occup. Environ. Med.*, 2008, **12**(2), 61.
2 T. D. Pham and B. K. Lee, Effects of Ag doping on the photocatalytic disinfection of E. coli in bioaerosol by Ag–TiO_2/GF under visible light, *J. Colloid Interface Sci.*, 2014, **428**, 24–31.
3 I. K. Panagopoulos, A. N. Karayannis, P. Kassomenos and K. Aravossis, A CFD simulation study of VOC and formaldehyde indoor air pollution dispersion in an apartment as part of an indoor pollution management plan, *Aerosol Air Qual. Res.*, 2011, **11**(6), 758–762.
4 S. Naghibi, S. Vahed, O. Torabi, A. Jamshidi and M. H. Golabgir, Exploring a new phenomenon in the bactericidal response of TiO_2 thin films by Fe doping: exerting the antimicrobial activity even after stoppage of illumination, *Appl. Surf. Sci.*, 2015, **327**, 371–378.
5 P. Sanitnon, S. Chiarakorn, C. Chawengkijwanich, S. Chuangchote and T. Pongprayoon, Synergistic effects of zirconium and silver co-dopants in TiO_2 nanoparticles for photocatalytic degradation of an organic dye and antibacterial activity, *J. Aust. Ceram. Soc.*, 2019, 1–2.
6 J. M. Herrmann, Heterogeneous photocatalysis: fundamentals and applications to the removal of various types of aqueous pollutants, *Catal. Today*, 1999, **53**(1), 115–129.
7 M. Anpo and M. Takeuchi, The design and development of highly reactive titanium oxide photocatalysts operating under visible light irradiation, *J. Catal.*, 2003, **216**(1–2), 505–516.
8 L. H. Huang, C. Sun and Y. L. Liu, Pt/N-codoped TiO_2 nanotubes and its photocatalytic activity under visible light, *Appl. Surf. Sci.*, 2007, **253**(17), 7029–7035.
9 H. F. Moafi, A. F. Shojaie and M. A. Zanjanchi, Photoactive behavior of polyacrylonitrile fibers based on silver and zirconium co-doped titania nanocomposites: synthesis, characterization, and comparative study of solid-phase photocatalytic self-cleaning, *J. Appl. Polym. Sci.*, 2013, **127**(5), 3778–3789.
10 N. Sobana, M. Muruganadham and M. Swaminathan, Nano-Ag particles doped TiO_2 for efficient photodegradation of direct azo dyes, *J. Mol. Catal. A: Chem.*, 2006, **258**(1–2), 124–132.
11 A. A. Ismail and H. Matsunaga, Influence of vanadia content onto TiO_2–SiO_2 matrix for photocatalytic oxidation of trichloroethylene, *Chem. Phys. Lett.*, 2007, **447**(1–3), 74–78.
12 N. Venkatachalam, M. Palanichamy and V. Murugesan, Sol–gel preparation and characterization of alkaline earth metal doped nano TiO_2: efficient photocatalytic degradation of 4-chlorophenol, *J. Mol. Catal. A: Chem.*, 2007, **273**(1–2), 177–185.
13 S. M. Chang and R. A. Doong, Characterization of Zr-doped TiO_2 nanocrystals prepared by a nonhydrolytic sol– gel method at high temperatures, *J. Phys. Chem. B*, 2006, **110**(42), 20808–20814.
14 B. Gao, T. M. Lim, D. P. Subagio and T. T. Lim, Zr-doped TiO_2 for enhanced photocatalytic degradation of bisphenol A, *Appl. Catal., A*, 2010, **375**(1), 107–115.
15 H. Zhang, Q. Tang, Q. Li, Q. Song, H. Wu and N. Mao, Enhanced Photocatalytic Properties of PET Filaments Coated with Ag-N Co-Doped TiO_2 Nanoparticles Sensitized with Disperse Blue Dyes, *Nanomaterials*, 2020, **10**(5), 987.
16 S. Naraginti, Y. Li and G. L. Puma, Photocatalytic mineralization and degradation kinetics of sulphamethoxazole and reactive red 194 over silver-zirconium co-doped titanium dioxide: reaction mechanisms and phytotoxicity assessment, *Ecotoxicol. Environ. Saf.*, 2018, **159**, 301–309.
17 A. Juma, I. O. Acik, A. T. Oluwabi, A. Mere, V. Mikli, M. Danilson and M. Krunks, Zirconium doped TiO_2 thin films deposited by chemical spray pyrolysis, *Appl. Surf. Sci.*, 2016, **387**, 539–545.

18 N. Bsiri, M. A. Zrir, A. Bardaoui and M. Bouaïcha, Morphological, structural and ellipsometric investigations of Cr doped TiO_2 thin films prepared by sol–gel and spin coating, *Ceram. Int.*, 2016, **42**(9), 10599–10607.

19 A. N. Banerjee, N. Hamnabard and S. W. Joo, A comparative study of the effect of Pd-doping on the structural, optical, and photocatalytic properties of sol–gel derived anatase TiO_2 nanoparticles, *Ceram. Int.*, 2016, **42**(10), 12010–12026.

20 V. S. Mohite, M. A. Mahadik, S. S. Kumbhar, Y. M. Hunge, J. H. Kim, A. V. Moholkar, K. Y. Rajpure and C. H. Bhosale, Photoelectrocatalytic degradation of benzoic acid using Au doped TiO_2 thin films, *J. Photochem. Photobiol., B*, 2015, **142**, 204–211.

21 F. Chekin, S. Bagheri and S. B. Abd Hamid, Synthesis of Pt doped TiO_2 nanoparticles: characterization and application for electrocatalytic oxidation of l-methionine, *Sens. Actuators, B*, 2013, **177**, 898–903.

22 W. Tongon, C. Chawengkijwanich and S. Chiarakorn, Visible light responsive Ag/TiO_2/MCM-41 nanocomposite films synthesized by a microwave assisted sol–gel technique, *Superlattices Microstruct.*, 2014, **69**, 108–121.

23 S. Krejčíková, L. Matějová, K. Kočí, L. Obalová, Z. Matěj, L. Čapek and O. Šolcová, Preparation and characterization of Ag-doped crystalline titania for photocatalysis applications, *Appl. Catal., B*, 2012, **111**, 119–125.

24 K. V. Bineesh, D. K. Kim and D. W. Park, Synthesis and characterization of zirconium-doped mesoporous nano-crystalline TiO_2, *Nanoscale*, 2010, **2**(7), 1222–1228.

25 G. Pansamut, T. Charinpanitkul and A. Suriyawong, Removal of humic acid by photocatalytic process: effect of light intensity, *Eng. J.*, 2013, **17**(3), 25–32.

26 A. Juma, I. O. Acik, A. T. Oluwabi, A. Mere, V. Mikli, M. Danilson and M. Krunks, Zirconium doped TiO_2 thin films deposited by chemical spray pyrolysis, *Appl. Surf. Sci.*, 2016, **387**, 539–545.

27 M. Ikram, S. Ali, R. Murray, A. Hussain and S. I. Shah, Influence of fullerene derivative replacement with TiO_2 nanoparticles in organic bulk heterojunction solar cells, *Curr. Appl. Phys.*, 2015, **15**(1), 48–54.

28 B. Duan, Y. Zhou, C. Huang, Q. Huang, Y. Chen, H. Xu and S. Shen, Impact of Zr-doped TiO_2 photocatalyst on formaldehyde degradation by Na addition, *Ind. Eng. Chem. Res.*, 2018, **57**(42), 14044–14051.

29 M. Aqeel, S. Anjum, M. Imran, M. Ikram, H. Majeed, M. Naz, S. Ali and M. A. Ahmad, TiO_2@ RGO (reduced graphene oxide) doped nanoparticles demonstrated improved photocatalytic activity, *Mater. Res. Express*, 2019, **6**(8), 086215.

30 A. Rafiq, M. Imran, M. Aqeel, M. Ikram, H. Majeed, S. G. Hussain and S. Ali, ZnS–Ni Doped Nanoparticles Served as Promising Nano-Photocatalyst (Industrial Dye Degrader), *Nanosci. Nanotechnol. Lett.*, 2019, **11**(8), 1060–1069.

31 U. Sattar, M. Ikram, M. Junaid, M. Aqeel, M. Imran and S. Ali, Annealing effect on synthesized ZnS/TiO_2 nanocomposite for treatment of industrial wastewater, *Mater. Res. Express*, 2019, **6**(11), 115050.

32 M. Junaid, M. Imran, M. Ikram, M. Naz, M. Aqeel, H. Afzal, H. Majeed and S. Ali, The study of Fe-doped CdS nanoparticle-assisted photocatalytic degradation of organic dye in wastewater, *Appl. Nanosci.*, 2019, **9**(8), 1593–1602.

33 P. Demircivi and E. B. Simsek, Fabrication of Zr-doped TiO_2/chitosan composite catalysts with enhanced visible-light-mediated photoactivity for the degradation of Orange II dye, *Water Sci. Technol.*, 2018, **78**(3), 487–495.

34 S. Naraginti, Y. Li and G. L. Puma, Photocatalytic mineralization and degradation kinetics of sulphamethoxazole and reactive red 194 over silver-zirconium co-doped titanium dioxide: reaction mechanisms and phytotoxicity assessment, *Ecotoxicol. Environ. Saf.*, 2018, **159**, 301–309.

35 T. Ali, A. Ahmed, U. Alam, I. Uddin, P. Tripathi and M. Muneer, Enhanced photocatalytic and antibacterial activities of Ag-doped TiO_2 nanoparticles under visible light, *Mater. Chem. Phys.*, 2018, **212**, 325–335.

36 A. Weibel, R. Bouchet, F. Boulc' and P. Knauth, The big problem of small particles: a comparison of methods for determination of particle size in nanocrystalline anatase powders, *Chem. Mater.*, 2005, **17**(9), 2378–2385.

37 H. C. Choi, Y. M. Jung and S. B. Kim, Size effects in the Raman spectra of TiO_2 nanoparticles, *Vib. Spectrosc.*, 2005, **37**(1), 33–38.

38 T. Ohsaka, Temperature dependence of the Raman spectrum in anatase TiO_2, *J. Phys. Soc. Jpn.*, 1980, **48**(5), 1661–1668.

39 S. Huang, Y. Yu, Y. Yan, J. Yuan, S. Yin and Y. Cao, Enhanced photocatalytic activity of TiO_2 activated by doping Zr and modifying Pd, *RSC Adv.*, 2016, **6**(36), 29950–29957.

40 D. P. Opra, S. V. Gnedenkov, S. L. Sinebryukhov, E. I. Voit, A. A. Sokolov, A. Y. Ustinov and V. V. Zheleznov, Zr^{4+}/F-co-doped TiO_2 (anatase) as high performance anode material for lithium-ion battery, *Prog. Nat. Sci.: Mater. Int.*, 2018, **28**(5), 542–547.

41 V. Swamy, Size-dependent modifications of the first-order Raman spectra of nanostructured rutile TiO_2, *Phys. Rev. B: Condens. Matter Mater. Phys.*, 2008, **77**(19), 195414.

42 W. F. Zhang, Y. L. He, M. S. Zhang, Z. Yin and Q. Chen, Raman scattering study on anatase TiO_2 nanocrystals, *J. Phys. D: Appl. Phys.*, 2000, **33**(8), 912.

43 A. Orendorz, A. Brodyanski, J. Lösch, L. H. Bai, Z. H. Chen, Y. K. Le, C. Ziegler and H. Gnaser, Structural investigation of pristine and annealed nanocrystalline TiO_2 thin films by X-ray diffraction and Raman spectroscopy, *Phys. Status Solidi C*, 2007, **4**(6), 1822–1829.

44 T. Ali, A. Ahmed, U. Alam, I. Uddin, P. Tripathi and M. Muneer, Enhanced photocatalytic and antibacterial activities of Ag-doped TiO_2 nanoparticles under visible light, *Mater. Chem. Phys.*, 2018, **212**, 325–335.

45 M. Manzoor, A. Rafiq, M. Ikram, M. Nafees and S. Ali, Structural, optical, and magnetic study of Ni-doped TiO_2 nanoparticles synthesized by sol–gel method, *Int. Nano Lett.*, 2018, **8**(1), 1–8.

46 A. N. Murashkevich, A. S. Lavitskaya, T. I. Barannikova and I. M. Zharskii, Infrared absorption spectra and structure of TiO_2-SiO_2 composites, *J. Appl. Spectrosc.*, 2008, **75**(5), 730.

47 K. Karthik, S. K. Pandian and N. V. Jaya, Effect of nickel doping on structural, optical and electrical properties of TiO_2 nanoparticles by sol–gel method, *Appl. Surf. Sci.*, 2010, **256**(22), 6829–6833.

48 R. Liu, H. S. Wu, R. Yeh, C. Y. Lee and Y. Hung, Synthesis and bactericidal ability of TiO_2 and Ag-TiO_2 prepared by coprecipitation method, *Int. J. Photoenergy*, 2012, **2012**, 640487.

49 J. Lukáč, M. Klementová, P. Bezdička, S. Bakardjieva, J. Šubrt, L. Szatmáry and A. Grusková, Characterization of Zr-doped TiO_2 prepared by homogenous co-precipitation without high-temperature treatment, *J. Mater. Sci.*, 2007, **42**(22), 9421–9428.

50 H. Zhang, Q. Tang, Q. Li, Q. Song, H. Wu and N. Mao, Enhanced Photocatalytic Properties of PET Filaments Coated with Ag-N Co-Doped TiO_2 Nanoparticles Sensitized with Disperse Blue Dyes, *Nanomaterials*, 2020, **10**(5), 987.

51 I. Singh, R. Kumar and B. I. Birajdar, Zirconium doped TiO_2 nano-powder via halide free non-aqueous solvent controlled sol-gel route, *J. Environ. Chem. Eng.*, 2017, **5**(3), 2955–2963.

52 N. Sobana, M. Muruganadham and M. Swaminathan, Nano-Ag particles doped TiO_2 for efficient photodegradation of direct azo dyes, *J. Mol. Catal. A: Chem.*, 2006, **258**(1–2), 124–132.

53 P. Goswami and J. N. Ganguli, Tuning the band gap of mesoporous Zr-doped TiO_2 for effective degradation of pesticide quinalphos, *Dalton Trans.*, 2013, **42**(40), 14480–14490.

54 K. V. Bineesh, D. K. Kim and D. W. Park, Synthesis and characterization of zirconium-doped mesoporous nano-crystalline TiO_2, *Nanoscale*, 2010, **2**(7), 1222–1228.

55 X. Wang, R. L. Patel and X. Liang, Significant improvement in TiO_2 photocatalytic activity through controllable ZrO_2 deposition, *RSC Adv.*, 2018, **8**(45), 25829–25834.

56 H. F. Moafi, A. F. Shojaie and M. A. Zanjanchi, Photoactive behavior of polyacrylonitrile fibers based on silver and zirconium co-doped titania nanocomposites: synthesis, characterization, and comparative study of solid-phase photocatalytic self-cleaning, *J. Appl. Polym. Sci.*, 2013, **127**(5), 3778–3789.

57 S. Naraginti, F. B. Stephen, A. Radhakrishnan and A. Sivakumar, Zirconium and silver co-doped TiO_2 nanoparticles as visible light catalyst for reduction of 4-nitrophenol, degradation of methyl orange and methylene blue, *Spectrochim. Acta, Part A*, 2015, **135**, 814–819.

58 Q. Huang, W. Ma, X. Yan, Y. Chen, S. Zhu and S. Shen, Photocatalytic decomposition of gaseous HCHO by $Zr_xTi_{1-x}O_2$ catalysts under UV-vis light irradiation with an energy-saving lamp, *J. Mol. Catal. A: Chem.*, 2013, **366**, 261–265.

59 I. Singh, R. Kumar and B. I. Birajdar, Zirconium doped TiO_2 nano-powder via halide free non-aqueous solvent controlled sol-gel route, *J. Environ. Chem. Eng.*, 2017, **5**(3), 2955–2963.

60 R. Zuo, G. Du, W. Zhang, L. Liu, Y. Liu, L. Mei and Z. Li, Photocatalytic degradation of methylene blue using TiO_2 impregnated diatomite, *Adv. Mater. Sci. Eng.*, 2014, **2014**, 170148.

61 S. G. Kumar and L. G. Devi, Review on modified TiO_2 photocatalysis under UV/visible light: selected results and related mechanisms on interfacial charge carrier transfer dynamics, *J. Phys. Chem. A*, 2011, **115**(46), 13211–13241.

62 Q. Chen, W. Shi, Y. Xu, D. Wu and Y. Sun, Visible-light-responsive Ag–Si codoped anatase TiO_2 photocatalyst with enhanced thermal stability, *Mater. Chem. Phys.*, 2011, **125**(3), 825–832.

63 S. Krejčíková, L. Matějová, K. Kočí, L. Obalová, Z. Matěj, L. Čapek and O. Šolcová, Preparation and characterization of Ag-doped crystalline titania for photocatalysis applications, *Appl. Catal., B*, 2012, **111**, 119–125.

64 D. Kapusuz, J. Park and A. Ozturk, Sol–gel synthesis and photocatalytic activity of B and Zr co-doped TiO_2, *J. Phys. Chem. Solids*, 2013, **74**(7), 1026–1031.

65 C. S. Kim, J. W. Shin, S. H. An, H. D. Jang and T. O. Kim, Photodegradation of volatile organic compounds using zirconium-doped TiO_2/SiO_2 visible light photocatalysts, *Chem. Eng. J.*, 2012, **204**, 40–47.

66 P. Sanitnon, S. Chiarakorn, C. Chawengkijwanich, S. Chuangchote and T. Pongprayoon, Synergistic effects of zirconium and silver co-dopants in TiO_2 nanoparticles for photocatalytic degradation of an organic dye and antibacterial activity, *J. Aust. Ceram. Soc.*, 2019, 1–2.

